Pergamon

Int. J. Heat Mass Transfer. Vol. 38, No. 6, pp. 979–987, 1995

0017-9310/95 $9.50+0.00

0017-9310(94)00225-8

Pool boiling heat transfer—II. Thickness of liquid macrolayer formed beneath vapor masses

T. KUMADA and H. SAKASHITA

Department of Nuclear Engineering, Faculty of Engineering, Hokkaido University, North 13, West 8, Kita-ku, Sapporo 060, Japan

(*Received* 15 *July* 1993 *and in final form* 20 *July* 1994)

Abstract—The macrolayer thickness was determined on the basis of the energy balance relation $q_{CHF} = \delta_l \rho_l H_{fg} f$, which was derived from the dryout model for liquids, proposed by Katto and co-workers. The critical heat flux (CHF) and the detachment frequency were measured on 20 mm diameter horizontal and vertical heated disks at pressures of 0.03–0.4 MPa with water, ethanol, methanol and acetone. Two semi-empirical correlations for the macrolayer thickness were derived by dimensional analysis of a model in which primary or coalesced bubbles form a macrolayer. The proposed correlations arrange the data of macrolayer thickness obtained from CHF measurements well.

1. INTRODUCTION

Haramura and Katto [1] proposed the model of CHF shown in Fig. 1. In this model a macrolayer is formed on the heated surface when vapor bubbles detach and is dried out just before their detachment at CHF (critical heat flux). The model also postulates that the liquid supply beneath a vapor bubble is blocked during its growth at high heat fluxes, and that the surface heat flux is steady and contributes to macrolayer evaporation. CHF or surface dryout occurs when the heat flux is high enough to evaporate the macrolayer before the detachment of the vapor bubbles. The energy balance yields

$$q_{CHF} = \delta_l \rho_l H_{fg} (1 - A_V/A_W) f \quad (1)$$

where f is the detachment frequency, δ_l the initial macrolayer thickness, A_W the surface area of heaters, and A_V the total bottom area of vapor stems. The vapor stems are produced when the bulk liquid comes into contact with a highly superheated surface. Haramura and Katto postulated the macrolayer thickness to be one-fourth of the Helmholtz instability wavelength at the stem interface. They further postulated that CHF is given by the Zuber correlation, and the initial macrolayer thickness of Haramura and Katto becomes

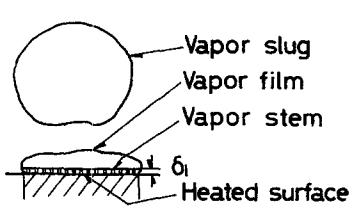

Fig. 1. Model of macrolayer formation proposed by Haramura and Katto.

$$\delta_l = 0.00536 \rho_V \sigma (\rho_V/\rho_l)^{0.4} (1 + \rho_V/\rho_l) (H_{fg}/q)^2. \quad (2)$$

Haramura and Katto stated that the idea of a vapor stem came from the experimental observations by Gaertner [6]. Contrary to this, Gaertner observed vapor stems not in the macrolayer at the start of formation, but in macrolayers which were thin enough not to produce bubbles by boiling.

Serizawa [2] presented a theoretical modeling of macrolayer formation at regular boiling CHF under power transients, and calculated CHF as a parameter of pressure and power transient. However, the model is based on a continuous liquid supply to the macrolayer, contradicting the physical evidence that there is none or very little liquid supply during the evaporation of the macrolayer.

Bhat *et al.* [3] proposed a mechanism of macrolayer formation. In their model primary bubbles grow and detach successively in each nucleation site, and form vapor stems by coalescence in a vertical direction. The radius of the vapor stems increases as the distance from the heated surface increases, and coalesce at some distance from the heated surface, forming macrolayers. They provided a set of differential equations, allowing a numerical calculation of the thickness of the macrolayer for water. The resulting initial macrolayer thickness for water at atmospheric pressure is

$$\delta_l = 1.59 q^{-1.527}. \quad (3)$$

Recently Pasamehmetoglu *et al.* [4] and Rajvanshi *et al.* [5] modified the model of Haramura and Katto. Rajvanshi *et al.* assumed that vapor jets are anchored to the solid wall and steadily nourished with vapor, as a liquid film including vapor stems (cause of instability) can exist stably up to a distance δ_l from the heated surface. This does not remove physically

NOMENCLATURE

a_l thermal diffusivity of liquid [$m^2 s^{-1}$]
b $N_{Ja} a_l^{1/2}$ [$m s^{-1/2}$]
C constant
C_{Pl} specific heat of liquid [$J kg^{-1} K^{-1}$]
D diameter of heating surface [m]
D_b diameter of bubbles [m]
D_e width of primary bubbles [m]
d_c diameter of dry spot [m]
f detachment frequency of bubbles [s^{-1}]
g gravity [$m s^{-2}$]
G_0 $q/(\rho_V H_{fg})$, blowing velocity of vapor [$m s^{-1}$]
H height of primary bubbles [m]
H_{fg} latent heat of evaporation [$J kg^{-1}$]
h_e height of plane to maximum diameter [m]
n density of nucleation sites [m^{-2}]
p system pressure [Pa]
q, q_{CHF} heat flux and critical heat flux [$W m^{-2}$]
r radius of bubbles [m]
R_P, R_C radius of primary and coalesced bubbles when coalescing simultaneously [m]
t time [s]
T_{sat} saturation temperature [K]
T_W wall temperature [K]
ΔT_{sat} superheat [K]
u_P, u_C radius growth rate of primary, coalesced bubbles [$m s^{-1}$].

Greek symbols
δ_l, δ_M mean thickness of macrolayer, microlayer [m]
$\delta_M(r)$ thickness of microlayer [m]
λ_l thermal conductivity of liquid [$W m^{-1} K^{-1}$]
μ_l viscosity of liquid [Pa s]
ν_l dynamic viscosity of liquid [$m^2 s^{-1}$]
ρ_V, ρ_l density of vapor and liquid [$kg m^{-3}$]
σ surface tension [$N m^{-1}$].

Dimensionless quantities
g^+ $gb^8\rho_l^3/\sigma^3$
N_{Ja} $\rho_l C_{Pl}\Delta T_{sat}/\rho_V H_{fg}$, Jakob number
Pr ν_l/a_l, Prandtl number of liquid
t^+ $t\sigma^2/(b^6\rho_l^2)$.

unsustainable conditions of the instability model of vapor stems of Haramura and Katto. Rajvanshi *et al.* provided a simplified correlation from correlation (2), of Haramura and Katto:

$$\delta_l = 0.0107\sigma\rho_V(\rho_V/\rho_l)^{0.4}(H_{fg}/q)^2. \quad (4)$$

Gaertner [6] observed macrolayers using an upward-facing 50 mm diameter horizontal disk and discussed the relation between the macrolayer thickness and the diameter of vapor stems in the macrolayer. Iida and Kobayasi [7] determined the thickness of the macrolayer by measuring the distribution of voids in the vicinity of the heating surface by a needle conduction probe. Bhat and Saini [8], Shoji [9] and Rajvanshi *et al.* [5] also measured the thickness of macrolayers with a conduction probe similar to that of Iida and Kobayasi. In most measurements the interface is determined by the position where the void fraction or fluctuation frequency changes drastically. The macrolayer thickness is determined from the distance between the interface and the heated surface. Shoji tried to measure the macrolayer thickness accurately, but the uncertainty in the data is very large. This low reliability of data is mainly due to the irregular motion at the interface between the vapor and liquid phases due to the violent boiling in the macrolayer. These measurements must, therefore, be compared with data from other methods of determining macrolayer thickness.

Kumada and Sakashita [10] and Sakashita and Kumada [11] proposed a mechanism of macrolayer formation where the macrolayer is formed by the coalescence of primary or coalesced bubbles, and derived the Kutateladze–Zuber CHF correlation. The CHF phenomena are expressed by a simplified correlation by neglecting A_V/A_W, which is small when compared with unity:

$$q_{CHF} = \delta_l\rho_l H_{fg} f. \quad (5)$$

If q_{CHF} and f are determined, then the macrolayer thickness δ_l at formation can be calculated with correlation (5), assuming that the macrolayer on the heater is completely dried out.

In this paper CHF and bubble frequency were measured at pressures of about 0.03–0.4 MPa with water, ethanol, methanol and acetone on a horizontal or vertical 20 mm diameter heating disk, where large vapor masses form and detach periodically. The thickness of the macrolayer is calculated with the present and previously reported data of CHF. The semi-empirical correlation for the case where the macrolayer is formed by the coalescence of primary or coalesced bubbles (secondary bubbles) was obtained by dimensional analysis, and compared with the macrolayer thicknesses obtained from the present and previously reported data of CHF.

2. EXPERIMENTAL

2.1. *Experimental apparatus and procedure*

Figure 2(a) shows a cross-section of the experimental setup with a horizontal disk. The heating sur-

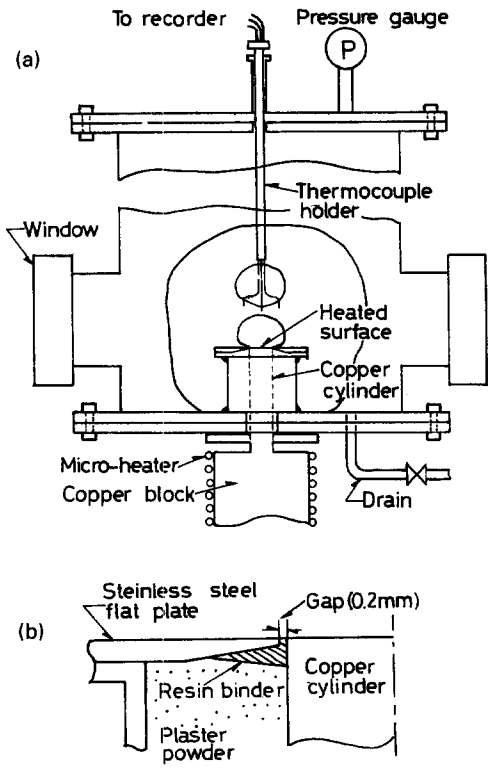

Fig. 2. (a) Experimental apparatus for boiling on horizontal and vertical disks. (b) Details of heating surface.

face is 20 mm in diameter and made of copper, placed in the central portion of the pressure vessel. To determine the thickness of the macrolayer correctly, a vapor mass must be large enough to cover the whole area of the heating surface. At CHF the blowing velocity of vapor G_0 decreases as the system pressure increases. With a 20 mm diameter heated disk, such a vapor mass forms when the vapor blowing velocity is above about 0.2 m s^{-1}. The experiment shows that the system pressure which attains such a vapor blowing velocity at CHF is below 0.4 MPa for water, 0.3 MPa for ethanol and methanol, and 0.25 MPa for acetone. The measurements were performed for pressures of 0.05–0.4 MPa for water, 0.03–0.3 MPa for ethanol, 0.05–0.24 MPa for methanol and 0.05–0.25 MPa for acetone.

Figure 2(b) shows details of the heating surface and its surroundings. For an upward heating surface of small diameter like this, CHF strongly depends on the structure of the joint between the edge of the disk and the surrounding plate. A silicone resin-filled gap of 0.3 mm was provided between the edge of the disk and the surrounding plate. A large 20 mm diameter disk was used to reduce the effect of the edge of the heating surface on CHF. The CHF and detachment frequency were also measured for a vertical disk, with the same experimental apparatus as shown in Fig. 2(a), inclined at 90°. Bubble frequency for the horizontal and vertical disks was determined from pictures obtained with high speed video images (max. 2066 f s^{-1}). For each measurement, boiling curves shift a few centigrade higher and the CHF increased by a few percent, within measurement errors. To plot the thickness of the macrolayer against the Jakob number it is necessary to know the superheat at CHF. This superheat was determined by the intersection between the extrapolation of the straight line of boiling curves and the horizontal line at CHF in the log q–log ΔT_{sat} plot.

2.2. *Calculation of macrolayer thickness*

To determine the macrolayer thickness accurately, the blowing velocity of vapor G_0 must be large enough to exceed the limit where the vapor mass covers the whole area of the heating surface. The vapor mass covering the whole area of the disk is formed at a blowing velocity above 0.2 m s^{-1} for the horizontal 20 mm diameter disk. At a 0.1–0.2 m s^{-1} blowing velocity range, a similar large vapor mass also formed on the heating surface and this vapor mass contained many incompletely coalesced small bubbles. Here, the data on bubble frequency for vapor blowing velocities above 0.15 m s^{-1} are used.

Near atmospheric pressure, bubble frequency at CHF can be correctly determined with horizontal and vertical disks smaller than 30 mm diameter. Where detachment frequencies are not given in reports where CHF was measured with disk heaters smaller than 30 mm diameter, the detachment frequency is calculated with the correlation for horizontal disks [17]:

$$f = 0.215\{g(\rho_l - \rho_v)/\rho_l\}^{5/9}/(\nu_l D^3)^{1/9}. \quad (6)$$

The thickness of the macrolayer was determined by substituting the measured values of CHF and the bubble frequency into correlation (5).

2.3. *Liquid flow into macrolayer during bubble growth*

When there is liquid flow into a macrolayer during bubble growth, the apparent thickness of the macrolayer calculated by correlation (5) becomes thicker than that which would be formed by simultaneous coalescence of bubbles. Katto and Yokoya [12] suggested that there is no liquid flow from the surroundings into a macrolayer during the growth of bubbles hovering above the heated surface at CHF, while there is liquid flow into the macrolayer in transition boiling.

In the present experiments the bubble behavior and the formation and evaporation process of the macrolayer were directly observed with a high speed video camera for the vertical disk, and it was confirmed that there is no liquid flow into the macrolayer during bubble growth. On the vertical heating surface, vapor masses periodically form and rise smoothly upwards. Vapor films are formed on the heating surface immediately when the liquid following vapor masses come into contact with the dried surface and grows to become vapor masses with vapor supplied from the evaporation of the macrolayer which forms under the

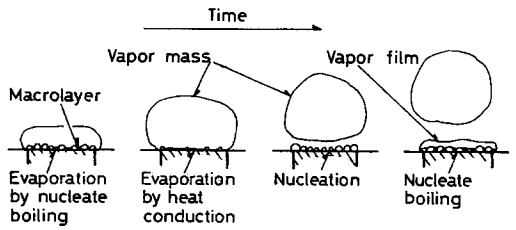

Fig. 3. Sketch showing behavior of vapor mass and macrolayer.

vapor film. Figure 3 is a sketch showing how vapor masses and macrolayers behave on the heating surface.

The consistency between macrolayer thicknesses for the horizontally and vertically oriented disk indirectly supports the fact that there is no liquid flow into the macrolayer on horizontal disks at CHF. Table 1 gives the measured conditions used here and the data sources.

2.4. *Macrolayer thickness vs Jakob number*

Figure 4 shows the macrolayer thickness vs Jakob number for various liquids from existing sources, as shown in Table 1. It is necessary to know the superheat of boiling surfaces at CHF to plot the data of macrolayer thickness vs Jakob number. The data from a conduction probe cannot be plotted, because these data are measured at heat fluxes below CHF and the superheat in measurement of heat flux are not given. Katto and Yokoya [18] provided a boiling curve under atmospheric pressure, but did not give boiling curves at low pressures. These boiling curves were estimated by the method proposed by Sakashita and Kumada [19], using a boiling curve at atmospheric pressure.

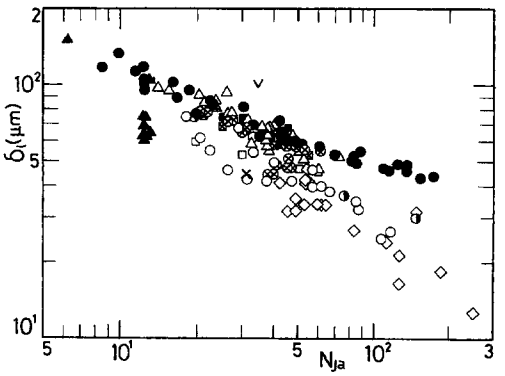

Fig. 4. Macrolayer thickness vs Jakob number.

The liquid nitrogen boiling curves of Kosty and Lyon [16] are used instead of the CHF data on nitrogen of Grigoriev and Klimenko [15], as they did not show boiling curves relevant to the CHF data. In Fig. 4, the macrolayer thickness decreases with increasing Jakob number, but does not correlate well with Jakob number.

2.5. *Ratio of macrolayer thickness to radius of primary bubbles*

(a) *Radius of primary bubbles.* The authors here propose a model of macrolayer formation where a macrolayer is formed by the coalescence of primary bubbles at lower pressures and of coalesced (secondary) bubbles at higher pressures.

If the primary bubbles simultaneously nucleate and grow uniformly, the radius of primary bubbles R_P and the density of nucleation sites n are related by how crowded the bubbles are:

Table 1. Measurement conditions of the data obtained here

Reference	Authors	Pressure [MPa]	Diameter [mm]	Liquid	Symbol
[18]	Katto and Yokoya	0.02–0.1	10	H_2O	◇
[7]	Iida and Kobayashi	0.1	20	H_2O	◇
[13]	Yasukawa	0.1	10	H_2O	◇
[14]	Honda and Nishikawa	0.1	8	H_2O	◇
[15]	Grigoriev and Klimenko	0.1	8–20	N_2	▲
[16]	Kosty and Lyon	0.1	19	N_2, O_2	▲ ◑
				Ar, CH_4	× v
	Present authors		Horizontal		
		0.05–0.4	20	H_2O	○
		0.03–0.3	20	C_2H_6O	●
		0.05–0.24	20	CH_4O	⊗
		0.05–0.25	20	C_3H_6O	△
		0.103	5	H_2O	◒
			Vertical		
			20	H_2O	□
			20	C_2H_6O	■
			20	CH_4O	⊠

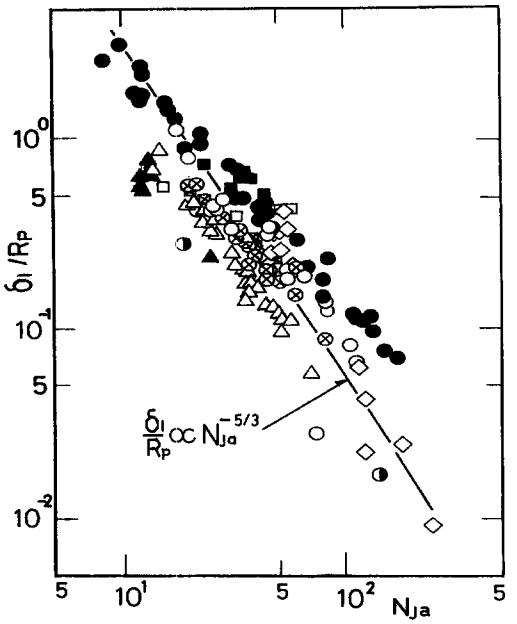

Fig. 5. Ratio of macrolayer thickness to radius of primary bubbles.

$$n\pi R_P^2 = 1. \quad (7)$$

The correlation relating the density of nucleation sites, heat flux, and superheat is given by Sakashita and Kumada [19] as

$$q = B_H \Delta T_{sat}^{4/3} n^{3/8} \quad (8)$$

where

$$B_H = 22.5\lambda_l Pr^{-0.2}\{g(\rho_l - \rho_v)/\sigma\}^{1/8} \times (\rho_l C_{Pl}/\rho_v H_{fg})^{1/3}. \quad (9)$$

The radius of primary bubbles can be obtained from correlation (8) using correlation (7), as

$$R_P = \pi^{-1/2} B_H^{4/3} \Delta T_{sat}^{16/9}/q^{4/3}. \quad (10)$$

(b) *The ratio* δ_l/R_P. Figure 5 shows the dimensionless thickness obtained from the δ_l/R_P ratio (the measured macrolayer thickness to the radius of primary bubbles), obtained by correlation (10) vs the Jakob number. With small Jakob numbers the δ_l/R_P ratio is much larger than unity, and this means that the thickness of the macrolayer is much thicker than the radius of the primary bubbles, because the shape of bubbles appears spherical or hemispherical, as discussed in Section 3, and as gravity does not control such small bubbles. As discussed in Section 3, this may be explained, as the bubbles forming the macrolayer are not primary bubbles but coalesced bubbles in the low Jakob number range of the present measurements.

3. MECHANISM OF MACROLAYER FORMATION

3.1. *Bubble behavior and mechanism of coalescence*

(a) *Under atmospheric or lower pressures.* With boiling experiments on a horizontal disk heater of 2–30 mm diameter, a single large bubble covering the heated surface of a disk detaches intermittently when the heat flux is from about half of CHF to CHF. Just after a large bubble has detached from the surface of the disk heater, liquid rushing onto the surface comes into contact with the dry area and the heater surface is speedly covered with liquid in the form of a very thin liquid layer (macrolayer). The repeatedly formed macrolayer on the heater evaporates quickly and at CHF most of the heater surface is dried out. When the liquid rushing onto the surface comes into contact with a dry area, a large amount of nucleation occurs simultaneously. The density of nucleation sites is equal to about 10^6–10^7 sites m^{-2} at CHF under atmospheric pressure for water [19]. In this case the shape of bubbles is close to hemispherical, as observed by Shoji [9], because the reaction of the liquid surrounding bubbles is superior to the surface tension acting on them. The photograghs show that some of the heated surface is covered with vapor film formed by direct coalescence of primary bubbles or by coalesced bubbles consisting of few primary bubbles.

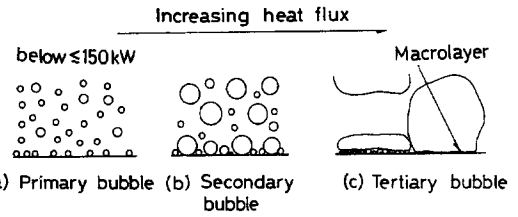

Fig. 6. Proposed model of macrolayer formation at moderate and higher pressures.

At lower pressures primary bubbles can grow to large diameters due to the small number of active sites, because the number of nucleation sites diminishes with p^2. The bubble diameter quickly grows and coalescence occurs simultaneously to produce oblate vapor films on the heated surface. The oblate vapor film grows with the vapor supplied by the macrolayer evaporation and detaches when it reaches a limiting size. Under low pressures each primary bubble has a wide microlayer below it: this means that most of the macrolayer consists of a microlayer and the thickness of the macrolayer is much smaller under lower pressures (larger Jakob number), as shown in Fig. 5.

(b) *Under moderate and high pressures.* At moderate and high pressures Semèria [20] measured the diameters of primary and coalesced bubbles in water on a horizontal 2 mm diameter cylinder and made photographic records. Based on the measurement of bubble diameters at detachment and the photographs of boiling at higher pressures by Semèria, it is possible to understand how bubbles behave under moderate and high pressures (refers to Fig. 6). The primary bubbles detach from the heating surface by convection liquid flow, when the heat flux is very small (below 150 kW m^{-2}). With increasing heat flux, the detachment of primary bubbles from the heating surface becomes difficult and they coalesce to become secondary

bubbles. The secondary bubbles move from the heating surface when buoyancy exceeds the various forces holding them to the heated surface. With further increase in heat flux, the increased bubble population and enlarged dry area at the bottom of the secondary bubbles cause them to stick to the heating surface and promote further coalescence. These coalesced bubbles are called tertiary bubbles. Due to their large size, the tertiary bubbles rest on a liquid macrolayer, formed by the coalescence of secondary bubbles.

3.2. *Shape of bubbles forming macrolayer*

Cooper *et al.* [21] observed the shape of bubbles with high-speed photographs under zero, 0.03 g, and normal gravity with water, toluene, and hexane. They measured four characteristic lengths: height H, bubble width D_e, the diameter of the dry spot at the bottom of bubbles d_e, and the thickness of the plane to maximum diameter h_e. The diameter of the bubbles was from 2 to 10 mm and the deformation was expressed by the ratio D_e/H. Values for D_e/H observed on the film were plotted against t^+. The shape of bubbles changes from hemispherical ($t^+ \fallingdotseq 0.2$) to spherical ($t^+ \fallingdotseq 1000$) in the $0.2 \leqslant t^+ \leqslant 1000$ range. The diameter of primary bubbles at CHF is smaller than 1.0 mm under atmospheric pressure for water on commonly used surfaces. The radius of primary bubbles is given by

$$R_P = CN_{Ja}^m (a_l t)^{1/2}. \tag{11}$$

When primary bubbles in water form a macrolayer at CHF and atmospheric pressure, if the diameter of bubbles $2R_P$ is 0.5 mm, the Jakob number 50, the constant C is 0.532, according to Okuyama [22], and the exponent of N_{Ja} in correlation (11) is 1, then it takes 1.61×10^{-3} s for bubbles to grow to a diameter of 0.5 mm. Here the value of t^+ becomes 14.8 and the bubble is somewhere between spherical and hemispherical. At CHF under atmospheric pressure, the shape of bubbles forming macrolayers of other liquids such as methanol, ethanol, and acetone is similar to that of water. The value of t^+ increases steeply with increasing system pressure as t^+ is proportional to $1/N_{Ja}^6$, and so the shape near atmospheric pressure changes from hemispherical to spherical with slightly increasing pressure or decreasing superheat for all the liquids. The shape of bubbles forming the macrolayer may change from hemispherical to spherical in the region expressed with $\delta_l/R_P \propto N_{Ja}^{-5/3}$ in Fig. 5.

3.3. *Effect of gravity on macrolayer formation*

Cooper *et al.* [21] measured the effect of gravity on the bubble size at detachment and provided the following relation for the condition of bubble detachment:

$$t_D^+ g^{+2/3} (= tg^{2/3}/N_{Ja}^{2/3} a_l^{1/3}) = 4. \tag{12}$$

Here t_D^+ is the dimensionless time at detachment of primary bubbles and g^+ is the dimensionless gravity. If the dimensionless time t^+, when bubbles form a macrolayer, is comparable to the dimensionless time t_D^+, the effect of gravity on the shape of bubbles cannot be neglected. The value of $t_D^+ g^{+2/3}$ for primary bubbles for various liquids at CHF and atmospheric pressure is much smaller than 4 ($t_D^+ g^{+2/3} \fallingdotseq 0.1$). This means that the effect of gravity on the shape of bubbles and the resulting thickness of the macrolayer may be neglected. If, as proposed in the next section, the macrolayer is formed by the coalescence of secondary bubbles at higher reduced pressures, the value of $t_D^+ g^{+2/3}$ for secondary bubbles becomes larger as the pressure increases. Here the effect of gravity on the shape of secondary bubbles cannot be neglected.

4. SEMIEMPIRICAL CORRELATION OF MACROLAYERS

4.1. *Macrolayer formation by primary bubbles*

The thickness of the macrolayer must be closely related to the diameter of bubbles forming the oblate vapor film, and depends on the strength of the various forces acting on the bubbles as well as the physical properties related to the bubble shape. The main forces acting on the bubbles are:

(a) reaction, F_R ($\propto \rho_l u_P^2$), from the rapid growth of bubbles which tends to keep them hemispherical; the inertia of liquid accompanying bubble growth and the reaction of the heating surface are expressed like F_R, if $\xi\rho_l + \rho_V$ is approximately ρ_l;

(b) surface tension, F_S ($\propto \sigma/R_P$), which tends to keep bubbles spherical;

(c) viscous force, F_V ($\propto \mu_l u_P/R_P$), from the viscosity of the liquid, which tends to prevent shape deformation, particularly when coalesced;

(d) buoyancy, F_B [$\propto 4R_P g(\rho_l - \rho_V)/3$], which draws bubbles in the direction opposite to gravity, but its contribution is small due to the small size of bubbles.

The ratio of these forces to F_R leads to the following three independent dimensionless parameters:

$$F_V/F_R = (\mu_l u_P/R_P)/(\rho_l u_P^2) = Pr/N_{Ja}^2 \tag{13}$$

$$F_S/F_R = (\sigma/R_P)/(\rho_l u_P^2) = (\sigma R_P)/(N_{Ja}^4 \rho_l a_l^2) \tag{14}$$

$$F_B/F_R = gR_P(\rho_l - \rho_V)/(\rho_l u_P^2) = gR_P^3(\rho_l - \rho_V)/(\rho_l N_{Ja}^4 a_l^2) \tag{15}$$

where it is assumed that primary bubbles grow according to relation (11) and that their growth rate is given by its differentiated form at time t:

$$u_P = (C/2)N_{Ja}(a_l/t)^{1/2} \tag{16}$$

where C is an unknown constant which can be empirically determined. It is assumed that the ratio between the macrolayer thickness and the radius of primary bubbles forming the macrolayer is expressed by

$$\delta_l/R_P = C(Pr/N_{Ja}^2)^i\{(\sigma R_P)/(N_{Ja}^4\rho_l a_l^2)\}^j \times \{gR_P^3(\rho_l-\rho_v)/(\rho_l N_{Ja}^4 a_l^2)\}^k. \quad (17)$$

The unknown constant C and the exponents i, j and k were empirically determined. When heat transfer is mainly attributed to heat conduction through the microlayer, the following relation is obtained:

$$q_l(r) = \{\lambda_l/\delta_M(r)\}\Delta T_{sat} \quad (18)$$

where $q_l(r)$ is the local heat flux by heat conduction at the distance r from the center of nucleation. The microlayer $\delta_M(r)$ is given by Cooper and Lloyd (1969) as

$$\delta_M(r) = C(Pr^{1/2}/N_{Ja})r. \quad (19)$$

Substituting equation (19) into equation (18) and integrating the relation about r from 0 to R_P gives

$$q = (1/\pi R_P^2)\int_0^{R_P} q_l(r)2\pi r\,dr$$

$$= \lambda_l\Delta T_{sat}/(C\,Pr^{1/2}\,R_P/2N_{Ja}) \quad (20)$$

$$= \lambda_l\Delta T_{sat}/\delta_M \quad (21)$$

where $\delta_M = C\,Pr^{1/2}\,R_P/2N_{Ja}$. From relation (20) the radius of primary bubbles becomes

$$R_P = (2/C)(\lambda_l/Pr_l^{1/2})(\rho_l C_{Pl}/\rho_v H_{fg})\Delta T_{sat}^2/q \quad (22)$$

$$= (2/C)(\lambda_l/Pr_l^{1/2})(N_{Ja}^2/\rho_l C_{Pl})/G_0. \quad (23)$$

Substituting equation (23) into equation (19), equation (17) becomes

$$\delta_l = C\,Pr^i\{\sigma/(\rho_l a_l^2)\}^j\{g(\rho_l-\rho_v)/(\rho_l a_l^2)\}^k \times (a_l/Pr^{1/2})^{j+3k+1}Na^{-2i-2j+2k+2}G_0^{-(j+3k+1)}. \quad (24)$$

Assuming that δ_l is independent of the superheat ΔT_{sat}, that is, $-2i-2j+2k+2 = 0$, then the result is

$$\delta_l = C[Pr^i(\rho_l a_l^2/\sigma)^{i-k-1}(a_l/Pr^{1/2})^{-i+4k+2} \times \{g(\rho_l-\rho_v)/(\rho_l a_l^2)\}^k]/G_0^{(-i+4k+2)} \quad (25)$$

where C and the exponents i and k are determined to fit the correlation with the data. At $C = 22.5, \delta \propto G_0^{-5/6}$, and $k = -1/10$,

$$\delta_l = 22.5[a_l^{25}\nu_l^{21}\sigma^8/\{\rho_l^2 g^6(\rho_l-\rho_v)^6\}]^{1/60}/G_0^{5/6}. \quad (26)$$

4.2. *Macrolayer formation by coalesced bubbles*

Under pressures fairly higher than atmospheric, large numbers of nucleation sites are activated and produce primary bubbles at very high frequencies. These bubbles quickly coalesce and produce larger bubbles, as shown in photographs by Seméria [20]. The boiling processes may cover most of the heated surface, because nucleation at higher pressures is possible even in the thin liquid layer under the bigger secondary bubbles. This allows the assumption that uniform vapor blowing takes place on the heated surface. In this case the bubbles grow according to the following relation:

$$d/dt\{(4\pi/3)r^3\} = \pi r^2 G_0 \quad (27)$$

where G_0 is the blowing velocity of vapor. The radius of bubbles at coalescence is expressed as

$$R_C = (1/4)G_0 t_C \quad (28)$$

where t_C is the time at coalescence after nucleation. The growth rate of bubbles is

$$u_C = (1/4)G_0. \quad (29)$$

Using relations (28) and (29), the ratios of the forces acting on the bubbles are expressed similarly to Section 4.1 as

$$F_V/F_R = (\mu_l u_C/R_C)/(\rho_l u_C^2) = \mu_l/(\rho_l G_0 R_C) \quad (30)$$

$$F_S/F_R = (\sigma/R_C)/(\rho u_C^2) = \sigma/(\rho_l G_0^2 R_C) \quad (31)$$

$$F_B/F_R = gR_C(\rho_l-\rho_v)/(\rho_l u_C^2) = gR_C(\rho_l-\rho_v)/(\rho_l G_0^2) \quad (32)$$

where the constants in relations (30)–(32) are neglected. It is also assumed that the ratio between the macrolayer thickness and the radius of the secondary bubbles forming the macrolayer is expressed by

$$\delta_l/R_C = C(\nu_l/G_0R_C)^i\{\sigma/(\rho_l G_0^2 R_C)\}^j \times \{g(\rho_l-\rho_v)R_C/(\rho_l G_0^2)\}^k. \quad (33)$$

The radius of coalesced bubbles may be determined by the relative magnitude of the forces acting on the bubbles as

$$C = (\nu_l/G_0R_C)^l(\sigma/\rho_l G_0^2 R_C)^m\{g(\rho_l-\rho_v)R_C/\rho_l G_0^2\}^n \quad (34)$$

where C is constant and R_C is expressed as

$$R_C = C(\nu_l/G_0)^{l/(m-n+l)}(\sigma/\rho_l G_0^2)^{m/(m-n+l)} \times \{g(\rho_l-\rho_v)/\rho_l G_0^2\}^{n/(m-n+l)}. \quad (35)$$

Substituting relation (35) into relation (33) and rearranging, we get

$$\delta_l = C(\nu_l/G_0)^x\{\sigma/(\rho_l G_0^2)\}^y \times \{g(\rho_l-\rho_v)/(\rho_l G_0^2)\}^{x+y-1} \quad (36)$$

where x and y are functions consisting of i, j, k, l, m and n. The data with δ_l, dependent on $G_0^{-5/6}$, then become

$$\delta_l = C\{\rho_l/g(\rho_l-\rho_v)\}^{7/24}(\sigma/\rho_l)^{17/24}[\nu_l(\rho_l/\sigma)^{3/4} \times \{g(\rho_l-\rho_v)/\rho\}^{1/4}]^x/G_0^{5/6} \quad (37)$$

where C and the exponent x are determined to fit the correlation best to the data. If $C = 0.786$ and $x = 1/3$, then

$$\delta_l = 0.786[\nu_l^8\sigma^{11}/\rho_l^6\{g(\rho_l-\rho_v)\}^5]^{1/24}/G_0^{5/6}. \quad (38)$$

4.3. *Gravity g in correlations* (26) *and* (38)

Gravity g appears in the denominator of correlations (26) and (38). It is difficult to assign a physical meaning to g here. The macrolayer thickness changes with variations in the forces acting on bubbles.

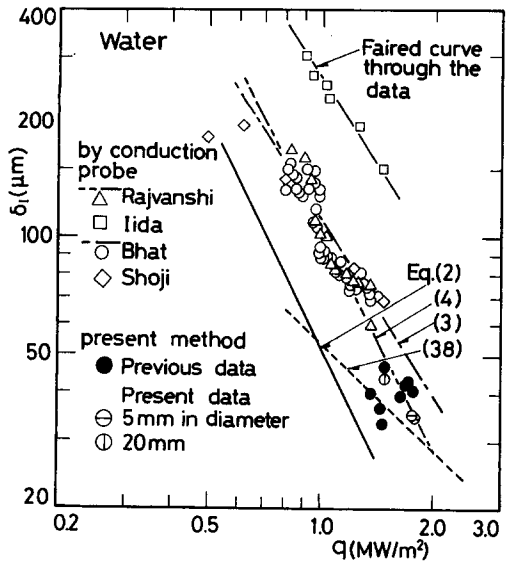

Fig. 7. Comparison of macrolayer thicknesses for water at atmospheric pressure.

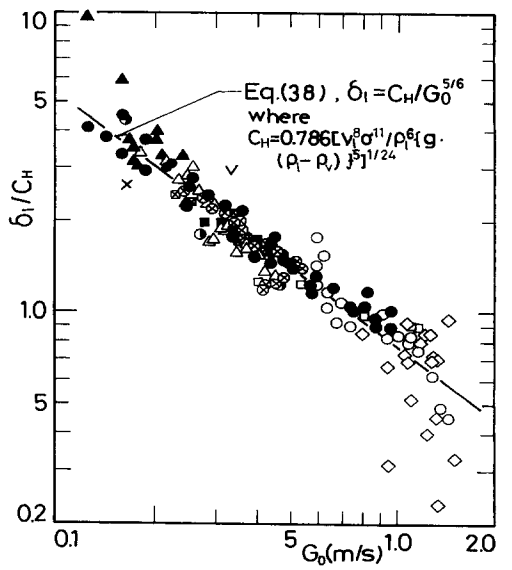

Fig. 9. Comparison of correlation (38) with data obtained here.

These forces continuously vary with variations in the blowing velocity G_0 at higher pressures, and the density of nucleation sites at lower pressures. This means that the macrolayer thickness cannot be expressed with one correlation like correlations (26) and (38). Correlations (26) and (38) are an average over 0.2 m $s^{-1} < G_0 < 1.0$ m s^{-1} for various liquids and pressures of 0.03–0.4 MPa. As a result the physical meaning of each term can not be defined strictly. The g in the denominator may be excluded, because the theoretical discussion shows that gravity is not significant in the macrolayer formation and there is no difference in the data obtained from horizontal and vertical heating surfaces. Further study will be required to discuss the effect of gravity on the behavior of bubbles forming the macrolayer.

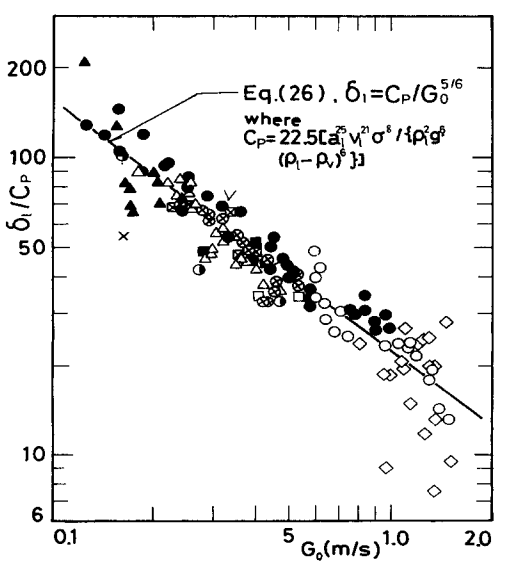

Fig. 8. Comparison of correlation (26) with data obtained here.

5. COMPARISON OF CORRELATIONS WITH EXPERIMENTAL DATA

5.1. *Data for water at atmospheric pressure*

Figure 7 shows a comparison of previously reported and the present experimental data with various semi-empirical correlations of the macrolayer thickness under atmospheric pressure. The modified correlation (4) by Rajvanshi *et al.* is much improved when compared with correlation (2), and it is consistent with all the data. The data of Iida and Kobayasi obtained at heat fluxes below CHF are somewhat larger than other data. The data of Shoji *et al.* are in fairly good agreement with those of Rajvanshi *et al.*, and the present data lie on a line extrapolated from the data of Shoji *et al.* and Rajvanshi *et al.* The macrolayer thickness of Bhat *et al.* and their correlation (3) are approximately proportional to $1/q^{3/2}$, while the correlations of Haramura and Katto and Rajvanshi *et al.* are proportional to $1/q^2$.

5.2. *Data from CHF*

Figures 8 and 9 show comparisons of measured macrolayers and calculations (26) and (38). The data arrangement in Fig. 9 seems to be a little better than that in Fig. 8, but the difference in both data arrangements is too small to determine which correlation is advantageous.

6. CONCLUSIONS

Boiling phenomena near CHF were discussed and a new model of macrolayer formation has been proposed. The macrolayer is formed by the coales-

cence of primary bubbles for larger Jakob numbers (relatively low pressure) and of secondary bubbles (coalesced bubbles) for smaller Jakob numbers (high pressure). The model of macrolayer formation is based on a dimensional analysis of various forces acting on the bubbles forming the macrolayer. The unknown constant and exponent in the derived correlation for the macrolayer were empirically determined with the present data as

$$\delta_l = 0.786[\nu_l^8\sigma^{11}/\{\rho_l^6 g^5(\rho_l-\rho_v)^5\}]^{1/24}/G_0^{5/6}.$$

The proposed correlation of macrolayer thickness arranges well the data obtained in the present measurements for water, methanol, ethanol, and acetone. The present model is developed from boiling phenomena at higher pressures, and the present correlation for macrolayer thicknesses can be applied to higher pressures for blowing velocities of $0.2\ \text{m s}^{-1} < G_0 < 1.0\ \text{m s}^{-1}$. For convenience, the correlation is in the form of a power function, and includes gravity, and will need further refinement with more experimental data.

REFERENCES

1. Y. Haramura and Y. Katto, New hydrodynamic model for critical heat flux (CHF), *Trans. JSME* **49**(445), 1919–1927 (1986) (in Japanese).
2. A. Serizawa, Theoretical prediction of maximum heat flux in power transients, *Int. J. Heat Mass Transfer* **26**, 921–931 (1981).
3. A. M. Bhat, R. Prakash and J. S. Saini, On the mechanism of macrolayer formation in nucleate boiling at high heat flux, *Int. J. Heat Mass Transfer* **26**, 735–740 (1986).
4. K. O. Pasamehmetoglu, R. A. Nelson and F. S. Gunnerson, Critical heat flux modeling in pool boiling for steady-state and power transients, *ASME J. Heat Transfer* **112**, 1048–1062 (1990).
5. A. K. Rajvanshi, J. S. Saini and R. Prakash, Investigation of macrolayer thickness in nucleate pool boiling at high heat flux, *Int. J. Heat Mass Transfer* **35**, 343–350 (1992).
6. R. F. Gaertner, Photographic study of nucleate boiling on a horizontal surface, *ASME J. Heat Transfer* **87**, 17–29 (1965).
7. Y. Iida and K. Kobayasi, An investigation on the mechanism of pool boiling phenomena by a probe method, *Proceedings of the 4th International Heat Transfer Conference*, Vol. 5, pp. 1–11 (1970).
8. A. M. Bhat and J. S. Saini, On the mechanism of macrolayer formation in nucleate pool boiling at high heat flux, *Int. J. Heat Mass Transfer* **26**, 833–840 (1983).
9. J. Shoji, A study of steady transition boiling of water: experimental verification of macrolayer evaporation model, *ASME Proceedings of the Engineering Foundation Conference on Pool and External Flow Boiling*, pp. 237–242 (1992).
10. T. Kumada and H. Sakashita, Proposed model for Kutateladze correlation and new correlation of CHF, *ASME Proceedings of the Engineering Foundation Conference on Pool and External Flow Boiling*, pp. 177–183 (1992).
11. H. Sakashita and T. Kumada, A new model for CHF in pool boiling at higher pressure, *JSME Int. J. Ser. B* **36**, 422–428 (1993).
12. Y. Katto and S. Yokoya, Behavior of vapor mass in saturated nucleate and transition pool boiling, *Heat Transfer Jap. Res.* **5**, 45–65 (1976).
13. Y. Yasukawa, Bubble behavior and temperature of heating surface near burnout point, *Trans. JSME* **43**(371), 2679–2686 (1977) (in Japanese).
14. H. Honda and K. Nishikawa, Study of boiling curve around transition boiling, *Trans. JSME* **34**(257), 177–184 (1972) (in Japanese).
15. V. A. Grigoriev and V. V. Klimenko, The influence of some heating surface properties on critical heat flux in cryogenic liquids boiling, *International Symposium of Heat and Mass Transfer*, Vol. PB-18, pp. 215–220 (1976).
16. P. G. Kosty and D. N. Lyon, Pool boiling heat transfer to cryogenic liquids, *A.I.Ch.E. Jl* 1265–1287 (1968).
17. T. Kumada, H. Sakashita and H. Yamagishi, Pool boiling heat transfer—I. Measurement and semi-empirical relations of detachment frequencies of coalesced bubbles, *Int. J. Heat Mass Transfer* **38**, 969–977 (1995).
18. Y. Katto and Y. Yokoya, Mechanisms of burnout and transition boiling in pool boiling, *Trans. JSME* **37**(295), 535–545 (1971) (in Japanese).
19. H. Sakashita and T. Kumada, Heat transfer correlation and method for predicting boiling curves of saturated nucleate boiling, *ASME Proceedings of the Engineering Foundation Conference on Pool and External Flow Boiling*, pp. 143–149 (1992).
20. R. Semèria, La cinématographie ultra-rapide et l'ébullition à haut pression, *La Houille Blanche* No. 6, 679–687 (1963).
21. M. G. Cooper, A. M. Judd and R. A. Pike, Shape and departure of single bubbles growing at a wall, *Proceedings of the 6th International Heat Transfer Conference, Toronto*, Vol. PB-1, pp. 115–120 (1978).
22. K. Okuyama, Transient boiling and enchancement of the limit of heat removal under large heat generation, Doctorate Thesis, Tokyo Institute of Technology (1983).